HHS Public Access

Author manuscript

*ACS Biomater Sci Eng*. Author manuscript; available in PMC 2019 January 08.

Published in final edited form as:

*ACS Biomater Sci Eng*. 2018 January 8; 4(1): 266–277. doi:10.1021/acsbiomaterials.7b00735.

# Hydroxylated Fullerene: A Stellar Nanomedicine to Treat Lumbar Radiculopathy via Antagonizing TNF-$\alpha$-Induced Ion Channel Activation, Calcium Signaling, and Neuropeptide Production

**Li Xiao**[†], **Kwangseok Hong**[‡], **Charles Roberson**[†], **Mengmeng Ding**[†], **Andrew Fernandez**[†], **Francis Shen**[†], **Li Jin**[†], **Swapnil Sonkusare**[‡,§], and **Xudong Li**[*,†,⊥]

[†]Department of Orthopaedic Surgery, Charlottesville, Virginia 22908, United States

[‡]Robert M. Berne Cardiovascular Research Center, Charlottesville, Virginia 22908, United States

[⊥]Department of Biomedical Engineering, University of Virginia, Charlottesville, Virginia 22908, United States

[§]Department of Molecular Physiology and Biological Physics, University of Virginia, Charlottesville, Virginia 22903, United States

## Abstract

Current nonsurgical treatments of discogenic lumbar radiculopathy are neither effective nor safe. Our prior studies have suggested that hydroxylated fullerene (fullerol) nanomaterial could attenuate proinflammatory cytokine tumor necrosis factor alpha (TNF-α)-induced neuroinflammation and oxidative stress in mouse dorsal root ganglia (DRG) and primary neurons. Here, we aim to investigate the analgesic effect of fullerol in a clinically relevant lumbar radiculopathy mouse model and to understand its underlying molecular mechanism in mouse DRGs and neurons. Surprisingly, single and local application of fullerol solution (1 $\mu$M, 10 $\mu$L) was sufficient to alleviate ipsilateral paw pain sensation in mice up to 2 weeks postsurgery. In addition, microCT data suggested fullerol potentially promoted disc height recovery following injury-induced disc herniation. Alcian blue/picrosirius red staining also suggested that fullerol promoted regeneration of extracellular matrix proteins visualized by the presence of abundant newly formed collagen and proteoglycan in herniated discs. For in vitro DRG culture, fullerol attenuated TNF-α-elicited expression of transient receptor potential cation channel subfamily V member 1 (TRPV-1) and neuropeptides release (substance P and calcitonin gene-related peptide). In addition, fullerol suppressed TNF-α-stimulated increase in intracellular $Ca^{2+}$ concentrations in primary neurons. Moreover, Western blot analysis in DRG revealed that fullerol's beneficial effects against TNF-α might be mediated through protein kinase B (AKT) and extracellular protein-regulated kinase (ERK) pathways. These TNF-α antagonizing and analgesic effects

[*]**Corresponding Author:** xl2n@virginia.edu. Tel: 1-434-924-5937. Fax: 1-434-924-1691.

**Supporting Information**

The Supporting Information is available free of charge on the ACS Publications website at DOI: 10.1021/acsbiomaterials.7b00735.

**ORCID**

Li Xiao: 0000-0003-1403-7472

**Notes**

The authors declare no competing financial interest.

indicated therapeutic potential of fullerol in treating lumbar radiculopathy, providing solid preclinical evidence toward further translational studies.

## Graphical abstract

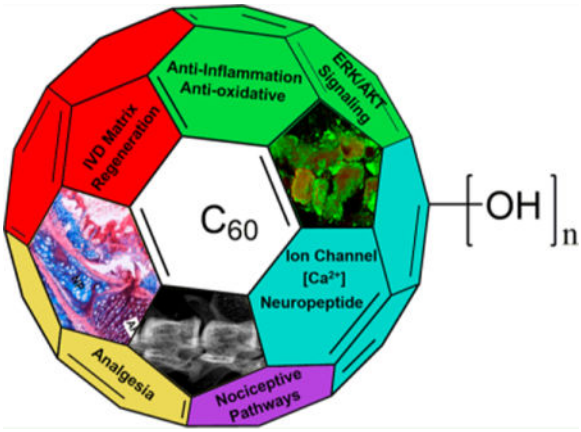


### Keywords

fullerene; radiculopathy; low back pain; ion channel; neuropeptide; disc herniation

## INTRODUCTION

Fullerene is a molecule of carbon in the form of a hollow sphere with diversified applications, such as photovoltaic and electronic devices, surface coating material, and antioxidant.[1] The original form of fullerene (also named $C_{60}$) is insoluble in water, impeding its biological applications.[2] On the basis of improved water solubility and biocompatibility, $C_{60}$-derivatives fullerol or fullerenol (hydroxylated fullerene) have been shown as promising therapeutic candidates against a range of pathological conditions involving oxidative stress and inflammation, such as cancer, diabetes mellitus, cardiovascular anomalies, neurodegeneration, skeletal muscle degeneration, osteoarthritis, and intervertebral disc degeneration.[2–4] In general, their beneficial biological effects could primarily be attributed to superior radical scavenging capabilities due to a cascade of downstream events initiated by excessive reactive oxygen species (ROS) production under oxidative stress. The cellular targets of these events might range from DNA to proteins to lipids. Given these research efforts, fullerol has been endowed as a next generation of antioxidant and anti-inflammatory materials. However, the majority of published results lack tissue- and disease-specific contextual investigation, which has hindered preclinical development and clinical translation of these promising pharmacologically active nanoparticles into nanomedicine.

The most recent *Global Burden of Disease* identified back and leg pain as the most common cause of disability worldwide with a prevalence of 80% and an estimated annual cost of $100 billion per year in the United States.[5,6] Although the pathogenesis of lumbar radiculopathy has not been fully elucidated, nerve compression and neuroinflammation play central roles.[7–10] Even as the most commonly used clinical treatment for lumbar

radiculopathy, epidural steroids injection has been reported to have various unexpected effects such as infection, allergic reaction, and malignancy.[11,12] TNF-α antagonists have emerged as a new therapy to treat inflammation-related chronic pain and sensory nerve damage.[13–15] However, a series of safety concerns have been raised regarding these TNF-α antagonists.[16–18] Therefore, there is an urgent medical need to discover a safe and effective therapy to treat lumbar radiculopathy and discogenic low back pain.[2] During the past 10 years, our laboratory has endeavored to explore the therapeutic potential and underlying mechanism of nanoparticle fullerol in the context of discogenic low back pain given such an unmet biomedical necessity. We previously demonstrated that intradiscal injection of fullerol solution effectively restored the extracellular matrix (ECM) content after disc injury in vivo and attenuated inducible nitric oxide synthase (iNOS) and interleukin-1 (IL-1) expression in disc cells in vitro.[19] Others have also demonstrated an antioxidative effect of fullerol in decreasing cellular and tissue damage following different stimuli.[3] Recently, we further revealed that fullerol inhibited disc material implantation-induced neuronal inflammation by regulating the nucleotide-binding oligomerization domain, leucine rich repeat and pyrin domain containing 3 (NLRP3) inflammasome activity and suppressing neurotropic peptide release in a nucleus pulposus (NP) implantation mouse model.[4] Additionally, fullerol has been shown to have a neuroprotective effect for both memory and neuronal damage through $Ca^{2+}$ signal transduction.[20] However, it is unclear whether and how fullerol possesses a therapeutic effect in a clinically relevant model that recapitulates herniation-caused radicular pain in humans.

In the current study, we present our preclinical findings in exploring mechanistic insights of fullerol as a pleiotropic nanomedicine therapeutic to treat lumbar radiculopathy. As shown in Figure 1, we hypothesize that fullerol antagonizes TNF-α-induced neuroinflammation in vitro, at least partially via suppressing (1) transient receptor potential cation channel subfamily V member 1 (TRPV-1) and intracellular $Ca^{2+}$ in dorsal root ganglion (DRG) neurons and (2) neuropeptides production and release from different sizes of neurons, contributing to an in vivo analgesic effect of a single administration of fullerol in our lumbar radiculopathy mouse model. A regenerative effect of fullerol was also observed in herniated discs. These therapeutic functions of fullerol might be attributed to downregulation of TNF-α-provoked phosphorylation of AKT and ERK pathways in both DRGs and macrophages. This report entails novel mechanistic understandings to support fullerol as a stellar nanomedicine in a lumbar radiculopathy and pain-specific pathological context, warranting further translational studies.

## MATERIALS AND METHODS

### Mouse Model of Lumbar Radiculopathy Secondary to Disc Herniation

The use of animals was approved by the Institutional Animal Care and Use Committee at the University of Virginia. Balb/C mice were purchased from Envigo (Indianapolis, IN; 8–10 weeks old, male 20–25 g) and housed in a 12 h light/dark cycle with free access to food and water. General anesthesia was induced with intraperitoneal injection of Ketamine/Xylazine (60–80/5–10 mg/kg). Briefly, using aseptic technique, the spine was exposed through an anterior midline transperitoneal approach with a surgical microscope. After separating the

hind peritoneum and psoas major muscle, L4 and L5 vertebrae were identified. The left L5 nerve root was exposed by removing the overlying psoas muscle fibers, and then the L4–5 disc was punctured laterally to enable nucleus protrusion toward the L5 nerve root. After surgery, animals were randomly assigned to two groups: injury + saline ($n = 5$) and injury + fullerol ($n = 5$). For the saline group, normal saline (10 $\mu$L) was added dropwise onto the herniated disc puncture. For the fullerol group, freshly prepared fullerol solution (10 $\mu$L, 1 $\mu$M in distilled and deionized water) was applied dropwise using a syringe onto the herniated disc. A sham-operated group ($n = 5$) with nerve exposure but without disc puncture was performed prior to the above surgeries to establish a baseline for mechanical hyperalgesia.

## Measurement of Mechanical Hyperalgesia (Pain Sensation)

For assessing the mechanical hyperalgesia of animals subjected to sham operation and disc herniation (with or without local fullerol treatment), electronic von Frey test was performed on both ipsilateral and contralateral hind paws for 3 consecutive days prior to surgery and every other day from postoperative day 1 (POD1) to POD12 in a blinded fashion following our prior publications.[1,4,21] In brief, mice were acclimated on an elevated mesh grid, and mechanical sensitivity was determined via the electronic von Frey apparatus as described.[22] Mechanical tests were measured 5 times for each paw with at least 5 min between tests on opposite paws and 10–15 min between tests on the same paw. For each paw, the mechanical thresholds from 3 trials were averaged after excluding the maximum and minimum readings. Both ipsilateral and contralateral mechanical thresholds were presented as mean ± SEM threshold values of each group presented for each time point.

## Microcomputed Tomography (MicroCT) Imaging and Disc Height Measurements

Two weeks following surgery, mice were euthanized in a $CO_2$ chamber, and spines were dissected and fixed in 10% formalin for 2 days. MicroCT scans ($n = 3$ per group) were performed on a microCT system (70 kV, 114 $\mu$A; microCT 80 scanner; Scanco Medical, Bassersdorf, Switzerland), which were then reconstructed with an isotropic voxel size of 10 $\mu$m. A multilevel thresholds procedure (threshold for bone = 205) was applied to discriminate vertebral column from disc. Three-dimensional images were acquired for qualitative and quantitative evaluation in an X-ray image mode. Heights of discs (L4–5 and L5–6) and vertebral bodies (L4, L5, and L6) were measured with ImageJ software by measuring lengths of a straight vertical line connecting anterior-to-anterior, midline-to-midline, and posterior-to-posterior sections of discs and vertebral bodies. The percentage disc height (PDH) was calculated as

$$\mathrm{PDH} = (\mathrm{d1} + \mathrm{d2} + \mathrm{d3})/(\mathrm{d1} + \mathrm{d2} + \mathrm{d3} + \mathrm{v1} + \mathrm{v2} + \mathrm{v3}) \quad (1)$$

for both L4–5 and L5–6 discs. A relative PDH ratio of L4–5 to L5–6 discs was then presented in which PDH of L5–6 was regarded as an internal control.[21]

## Alcian Blue/Picrosirius Red Staining

After fixation, spines were decalcified in 0.25 M EDTA for 2 weeks.[23] Paraffin-embedded sections (7 $\mu$m) were subjected to 1% alcian blue solution (pH 2.5) and picrosirius red (0.1%

sirius red in saturated aqueous picric acid) to visualize disc structure and ECM following published protocols.[21,24]

## Isolation of Primary Neurons from Dorsal Root Ganglia

In brief, mice were sacrificed in a $CO_2$ chamber followed by cervical dislocation. The bilateral DRGs were immediately collected from the spinal column of Balb/C mice (male and female, 8–12 wks, 20–25 g, Envigo, Indianapolis, IN) following our previously published protocols[3,4,21] and cultured in growth medium containing F-12 medium, 10% FBS, 100 U/mL penicillin, 100 μg/mL of streptomycin, and 10 ng/mL of nerve growth factors (NGF) (BD Biosciences, San Jose, CA). Cell culture supplies, F-12 nutrient mixture, fetal bovine serum (FBS), Dulbecco's phosphate-buffered saline (DPBS), penicillin-streptomycin, and Hank's balanced salt solution (HBSS, free of $Ca^{2+}$ and $Mg^{2+}$) were purchased from Life Technologies (Grand Island, NY). Other chemicals and solvents were purchased from Sigma-Aldrich (St. Louis, MO) unless otherwise specified.

Primary neurons were isolated from freshly harvested DRGs following published protocols with minor modifications.[3,21,25] Briefly, DRGs (20–30) were digested in 3 mL of papain (40 U/mL, in HBSS) (Worthington Biochemical Corporation, Lakewood, NJ) solution at 37°C for 10 min and centrifuged, and the upper solution was replaced with 3 mL of collagenase (0.2% in HBSS) (SERVA Electrophoresis GmbH, Heidelberg, Germany) and incubated at 37°C for 20 min. FBS (10%) was added to stop enzyme activity. The cell pellet was resuspended with 1 mL of complete growth medium containing F-12 medium, 10% FBS, 100 U/mL penicillin, and streptomycin. After gentle pipetting, dissociated cells were seeded onto poly-D-lysine/laminin-coated coverslips (BD Biosciences, San Jose, CA) in 24 well plates at a density of $1 \times 10^4$ cells/$cm^2$ and 80 μL of cell suspension per coverslip. After 2 h, cells were flooded with warm growth medium and cultured for 1 week until use. Fresh media was replaced on the second and fifth day after seeding.

## In Vitro Culture Protocol of Dorsal Root Ganglia Explants

Two days after DRG in vitro culture, serum-free growth medium was supplemented with TNF-α (Cell Signaling Technology, Danvers, MA, 25 ng/mL) with or without fullerol (MER Corp., Tucson, AZ) solution (1 μM, dissolved in distilled and deionized water). DRGs were harvested at different time points.

## Immunofluorescence Staining

Three combinations of dual-marker immunofluorescence staining (TRPV1–1/Pan neuron, substance P/Pan neuron, and CGRP/Pan neuron) were performed on DRG sections treated with or without TNF-α and TNF-α + fullerol (1 μM) for 24 h. After fixation in 4% PFA for 30 min at room temperature, DRGs were soaked in sucrose (15% then 30%), O.C.T embedded, and cryosectioned (5 μm). Then, DRG sections were permeabilized with 0.3% Triton X−100 in PBS for 10 min, blocked with 3% bovine serum albumin (BSA) in PBS, and incubated with mouse monoclonal substance P (SP) antibody (1:200) (R&D Systems, Minneapolis, MN), mouse monoclonal calcitonin gene-related peptide (CGRP) antibody (1:2000) (Sigma, a kind gift from Dr. Erisir at the University of Virginia), or goat polyclonal VR-1 (P-19) antibody (1:250) (TRPV-1, Santa Cruz Biotechnology, Dallas, TX) at 4°C

overnight and detected with either an Alexa Fluo594 goat-antimouse IgG (1:1000, Life Technologies) or a Rhodamine-conjugated donkey antigoat IgG (1:1000) and incubated at room temperature for 1 h. Subsequently, all sections were incubated with Neuro-Chrom Pan neuronal marker rabbit antibody (a polyclonal antibody blend that reacts against key somatic, nuclear, dendritic, and axonal proteins distributed across the Pan neuronal architecture, 1:250, EMD Millipore, Billerica, MA) at 4°C overnight to label neurons, detected by an FITC-labeled goat-anti-rabbit IgG (1:1000), and mounted with Prolong Gold antifade reagent (with DAPI) (Life Technologies). IgG control staining was performed following identical procedures excluding the primary antibodies. Representative fluorescence images were taken with an Olympus FV300 confocal laser scanning microscope (Olympus, Center Valley, NJ, USA) with the same settings among treatment groups.[26]

## Quantitative Analysis on Immunofluorescence Images

For quantification purposes, batch images were taken to capture the expression of TRPV-1, CGRP, substance P, and Pan neuronal markers of DRGs subjected to various treatments using a Nikon Eclipse E600 fluorescence microscope and a Nikon DS Ri2 camera. Using NIS-Elements software (Nikon), an exposure and gain combination was determined empirically for each target protein on FITC and TRITC filters, respectively (FITC for Pan, TRITC for VR-1, SP and CGRP) to ensure the dimmest regions of tissue were discernible visually for tracing without oversaturating the brightest regions.[27] At 200×, DRG tissues were imaged in three setting modes (VR-1/Pan, SP/Pan, CGRP/Pan). All cells expressing visually discernible Pan neuronal marker were marked as Pan-positive without differentiating their level of expression using the cytoplasmic gray values. When only displaying the Pan-positive (FITC channel) cells, boundaries of nucleated Pan-positive cells were manually traced followed by analysis on individual cell areas (in $\mu m^2$) and cytoplasmic mean gray values (0–255) with built-in software tools. When switching the display to the TRITC channel, cytoplasmic gray values on visually red and discernible cells were then analyzed and sorted by intensity from lowest to highest. The 30 lowest gray values were averaged to obtain a baseline intensity and subtracted from measured mean intensities. For each target, only cells with normalized intensities of 2.5-fold more than baseline were counted as positive expression. For TRPV-1, frequencies of TRPV-1/Pan neurons were summarized for small (<300 $\mu m^2$), medium (300− 700 $\mu m^2$), and large (>700 $\mu m^2$), and the frequencies of SP/Pan and CGRP/Pan neurons were sequentially analyzed in all neurons regardless of size. Neurons were size-categorized based on published consensus.[28]

## Enzyme-Linked Immunosorbent Assay (ELISA)

After 24 h of in vitro culture, the supernatant of DRG explant culture was collected to analyze the contents of substance P with an ELISA kit (R&D Systems, Minneapolis, MN) per the manufacturer's instructions.

## Western Blotting

DRGs (5–6/group) were lysed in 0.1 mL of lysis buffer (RIPA buffer supplemented with 1× proteinase inhibitor cocktail and PMSF). Lysates were subjected to SDS-PAGE and transferred to a nitrocellulose membrane. After incubation with Odyssey blocking buffer

(LI-COR, Lincoln, NE) for 1 h at room temperature, membranes were incubated with mouse phospho-ERK1/2 (1:1000) (Cell Signaling, Danvers, Massachusetts), rabbit total ERK 1/2 (1:1000) (Cell Signaling), rabbit phosphor-Akt1/2/3 (1:1000) (Santa Cruz Biotechnology, Dallas, TX), and rabbit total Akt1/2/3 (1:1000) (Santa Cruz Biotechnology) antibodies overnight at 4°C followed by incubation with a goat antimouse Alexa Fluo680 (1:5000) or goat antirabbit Alexa Fluo800 (1:5000) (ThermoFisher Scientific) for 1 h at room temperature. Membranes were scanned and analyzed.

## $Ca^{2+}$ Imaging and Estimation of Intracellular Global $Ca^{2+}$ Concentration

Primary neurons were isolated from mouse DRGs and seeded onto glass-bottom culture dishes (#0 cover glass, MatTek Corporation, Ashland, MA) and cultured for 6 days, as we previously published.[3,21] Cultured neurons were then treated with F-12 media (control), fullerol (1 $\mu$M), and TNF-α (10 ng/mL) with or without fullerol (1 $\mu$M) overnight and then incubated with a fluorescent $Ca^{2+}$ indicator Fluo-4 AM (10 $\mu$M) (Thermo Fisher Scientific) mixed with pluronic acid (0.04%) at 30°C for 30 min in the dark to measure intracellular global $Ca^{2+}$ fluorescence. Global $Ca^{2+}$ signals in neurons were imaged using an Andor Revolution WD (with Borealis) spinning-disk confocal imaging system (Andor Technology, Belfast, UK) that consists of an upright Nikon microscope with a 60× water-dipping objective (NA 1.0) and an electron-multiplying CCD camera, as previously described.[29,30] Images were recorded with Andor Revolution TL acquisition software (iQ3, Andor Technology) at 30 frames $s^{-1}$. Fluorescent probe-bound $Ca^{2+}$ was detected by exciting at 488 nm with a solid-state laser and collecting emitted fluorescence using a 525/36 nm bandpass filter. KCl solution (60 mM) was applied to induce membrane depolarization and assess voltage-dependent $Ca^{2+}$ influx. After removal of KCl solution, 20 mM extracellular $Ca^{2+}$ and 10 $\mu$M ionomycin (a membrane-permeable $Ca^{2+}$ ionophore) were applied to obtain maximal $Ca^{2+}$ fluorescence. $Ca^{2+}$ imaging experiments were performed at room temperature. Arbitrary global $Ca^{2+}$ fluorescence intensity was obtained by manually drawing an outline around 20–30 neurons within three randomly selected regions per treatment. The background fluorescence was then subtracted from the observed fluorescence. The fluorescence intensity collected from each neuron was averaged over a field of view. The arbitrary $Ca^{2+}$ fluorescence levels were evaluated using custom-designed SparkAn software (developed by Dr. Adrian Bonev, University of Vermont). Intracellular global $Ca^{2+}$ concentration ($[Ca^{2+}]_i$) in neuron cells was estimated using the following equation, as described previously[31,32]

$$[Ca^{2+}]_i = [K_d(F/F_{max} - 1/R_f)]/(1 - F/F_{max}) \quad (2)$$

where $K_d$ represents the Fluo-4 dissociation constant that is 340 nM, $F$ indicates an arbitrary fluorescence intensity at any given time during the recording, and $F_{max}$ is the maximal fluorescence intensity obtained in the presence of 20 mM extracellular $Ca^{2+}$ and 10 $\mu$M ionomycin. $R_f$ is 100 and represents the ratio of the $Ca^{2+}$ dye fluorescence at saturation in vitro relative to the zero $Ca^{2+}$ concentration.

### Statistical Analysis

For in vitro experiments, data obtained from three biological and three technical replicates were analyzed and presented as mean ± SEM. Repeated measurement one-way ANOVA was used to analyze pain data using GraphPad Prism software (GraphPad Software, Inc.). Data comparing two groups were analyzed with Student's *t* test. A chi-square test (Bonferroni posthoc test) was performed on the immunofluorescence quantitative data. Effect size of in vivo pain behavior study was conducted using mean and standard deviation based on Cohen's *d* calculation. A *p*-value of less than 0.05 was considered statistically significant.

## RESULTS

### Single Intraoperative Application of Fullerol Alleviated Mechanical Hyperalgesia in a Mouse Model of Lumbar Radiculopathy

Recently, our laboratory established a radiculopathy mouse model induced by lumbar disc herniation to mimic the human condition.[21] Using this model, mechanical sensitivity (von Frey) of each animal was evaluated every other day for up to 12 days postsurgery ($n = 5$ per group). Animal body weights were monitored in both injury and injury + fullerol groups to assess postsurgery recovery. Saline was used in the injury-only group as a control vehicle. As shown in Figure 2A, body weights slightly decreased (10–15%) within four days postsurgery and gradually recovered. No detectable difference in body weight was noted between the two groups. For sham-operated groups, a steady mechanical sensitivity could be detected in both ipsilateral and contralateral sides without a significant difference for up to POD12 compared to presurgery measurement (Figure 2B). As early as POD4, single intraoperative fullerol treatment effectively alleviated the mechanical hyperalgesia caused by disc herniation to a presurgery level in the ipsilateral side ($^{*}p < 0.05$ vs saline group) (Figure 2C). The mean mechanical threshold of the injury + fullerol group was significantly higher than that of the saline group ($p < 0.005$) with a large effect size (Cohen's $d > 2.0$). In contrast, the contralateral threshold of fullerol and saline groups showed no significant difference at all time points compared to the presurgery baseline (Figure 2D). Surprisingly, a single intraoperative application of fullerol at a relative low concentration and small amount (1 μM, 10 μL) improved the overall pain behavior of disc injured animals and further resulted in stronger hind leg muscle strength and more swift movement as observed in the Supplemental Video at POD4.

### Fullerol Potentiated Disc Regeneration in Herniated Mouse Discs

MicroCT images (Figure 3A) suggested that fullerol restored injury-induced disc height reduction by ~40% in the injured L4–5 discs compared to that of the saline group ($^{**}p = 0.0018$ for injury vs injury + fullerol) (Figure 3B). Alcian blue and picrosirius red with hematoxylin counter staining was further performed on harvested spines to examine structural, cellularity, and extracellular matrix change of injured mouse IVD with or without fullerol treatment.[33] Such staining provides a distinct visualization of both collagen (red) and proteoglycans (blue) and cellular components on the same histology section. As shown in Figure 3C, injured mouse IVD (middle row) underwent classical degenerative structural changes 2 weeks after injury, including an unclear boundary between annulus fibrosus (AF) and NP regions, enlarged and proliferated chondrocytes within the NP region, and disrupted

AF lamina when compared to the adjacent intact control IVD (top row). A single fullerol application resulted in an increased formation of collagen and proteoglycan (dark purple due to combination of blue and red) in the inner AF zone and increased collagen (red) synthesis in the outer AF layers (Figure 3C, bottom row) when compared to saline group, indicating a potential regenerative process.

## Fullerol Reversed TNF-α-Induced Alternation of TRPV-1 Expression in DRG Organ Culture

Subpopulations of DRG neurons exhibit different molecular characteristics, have specific peripheral and central targets, and require different target-derived trophic factors for their survival, differentiation, and maintenance.[34] It has been documented that small- and medium-sized DRG neurons are more responsive to non-noxious heat and chemical stimuli and express TRPV1.[34] TRPV-1 belongs to the vanilloid receptor family that can be activated by a diverse range of stimuli, including heat, protons, lipids, phorbols, phosphorylation, changes in extracellular osmolarity and/or pressure, and depletion of intracellular $Ca^{2+}$ stores. As novel pharmacological targets, the vanilloid receptors have potential in the development of many future disease treatments.[35] To understand whether (1) TNF-α could alter the TRPV-1 expression on various-sized mouse DRG neurons and (2) fullerol acted on such TNF-α-induced TRPV-1 alternation to alleviate the neuropathic pain in our model, we performed double immunofluorescence staining with Pan neuronal marker and TRPV-1 on DRG tissues (Figure 4A). Among all treatment groups (control, TNF-α, TNF-α + fullerol), total neurons (green) and TRPV-1-positive neurons (red) are listed based on neuron size in Figure 4B. Consistent with others studies, Pan neuronal marker staining depicted small (<300 $\mu m^2$, 60–70%) and medium (300–700 $\mu m^2$, 30–35%) neurons constituting the majority of mouse DRG neurons, whereas large neurons constituted less than 3% in all groups (Figure 4C). As shown in Figure 4D, when stimulated with TNF-α for 24 h, mouse DRGs expressed significantly higher levels of TRPV-1 in both small-and medium-sized neurons ($^{****}p < 0.0001$ vs control), whereas such elevation of %TRPV-1/Pan was markedly attenuated when cotreated with fullerol at 1 μM ($^{****}p < 0.0001$ vs both control and TNF-α groups).

## Fullerol Attenuated the TNF-α-Induced Increase in Global $Ca^{2+}$ Concentration $[Ca^{2+}]_i$ in Primary DRG Neurons

TNF-α has been implicated in many inflammatory disorders causing pain, including its alternation in numerous ion channels, especially $Ca^{2+}$ entry channels. It is believed that the increase in intracellular $[Ca^{2+}]_i$ indirectly leads to the release of certain neurotransmitters associated with pain, including CGRP[36] and substance P.[37] To explore fullerol's function in modulating $[Ca^{2+}]_i$ intercalated with TNF-α-evoked alternations in primary neurons, we demonstrated representative $Ca^{2+}$ fluorescence signals of neurons subject to various pretreatments (control, fullerol, TNF-α, and TNF-α + fullerol) under the basal conditions or following 60 mM KCl (Figure 5A). Intracellular $Ca^{2+}$ concentration for each group was quantitatively estimated in the absence or presence of 60 mM KCl (Figure 5B). Consistent with previous studies,[38] TNF-α pretreatment significantly increased $[Ca^{2+}]_i$ in primary DRG neurons ($^{*}p < 0.05$ vs control). Interestingly, whereas fullerol pretreatment alone did not alter basal $Ca^{2+}$ signaling, fullerol markedly suppressed the TNF-α-mediated increase in $[Ca^{2+}]_i$ at the baseline ($^{\#}p < 0.05$ vs TNF-α). In addition, 60 mM KCl was applied to test the

hypothesis that the fullerol negatively regulates $Ca^{2+}$ influx (Figure 5A and B). The high level of external $K^+$ elevated $[Ca^{2+}]_i$ in all groups, which was considerably diminished in neurons pretreated with fullerol or TNF-α + fullerol ($^{\dagger}p < 0.05$). Taken together, it is implicated that fullerol might alleviate neuropathic pain through modulating $Ca^{2+}$ signaling in DRG primary neurons.

## Fullerol Decreased TNF-α-Induced Neuropeptide Release in DRG Culture

Expression of neuropeptides substance P and CGRP in neurons are induced or upregulated following inflammation and considered a signal of neuronal damage, secreted to induce repair mechanisms and supportive glial reactions.[39] For substance P and CGRP expression to be visualized in different neurons of DRGs, double immunofluorescence staining is shown in Figure 6A and B. The frequencies of substance P- and CGRP-positive neurons were calculated and normalized by total neurons across three groups. As shown in Figure 6C, the percentage of CGRP immunopositive cells (red) was increased significantly in DRG tissue compared to the control ($^{*****}p < 0.05$ vs control) and returned to the basal level upon treatment with 1 μM fullerol ($^{\#\#\#\#}p < 0.0001$ vs TNF-α, n.s. vs control). The elevation of TNF-α-induced substance P was not as dramatic as CGRP, although fullerol significantly decreased both TNF-α elicited ($^{\#\#\#\#}p < 0.0001$) and basal control substance P expression ($^{*}p < 0.05$) (Figure 6D). Such increase in secreted substance P in culture media of DRG explants stimulated by TNF-α was also confirmed by ELISA ($^{*}p < 0.05$ vs control), which was robustly inhibited by fullerol at 1 μM ($^{\#}p < 0.05$ vs TNF-α) (Figure 6E). These results provided both qualitative and quantitative evidence of fullerol's effect on antagonizing TNF-α-elicited neuropeptide synthesis and release.

## Fullerol Attenuated TNF-α-Induced Activation of AKT and ERK in Both Cultured DRG and Macrophages

Mounting evidence supports the idea that ERK and AKT pathways are closely associated with TNF-α signaling, TNF-α-induced TRPV-1 expression, and potential mechanisms of anti-inflammatory therapeutics, in particular, in the context of neuronal signal transduction and nociception.[21,40–42] First, we tested TNF-α-induced time-dependent activation of AKT and ERK in DRGs and found the highest phosphorylation levels of both AKT and ERK at 5 h post TNF-α treatment (Figure S1). Therefore, we selected the 5 h time point to study the fullerol's effect on the phosphorylation levels of these proteins. As shown in Figure 7A–D, TNF-α dramatically elevated phosphor-AKT and ERK ($^{**}p < 0.01$ vs control) by 5- and 7-fold, respectively, whereas 1 μM of fullerol treatment significantly downregulated TNF-α-induced AKT and ERK phosphorylation ($^{\#}p < 0.05$ vs TNF-α and n.s. vs Control). These results indicated fullerol's effect on antagonizing TNF-α-induced neuroinflammation in DRG possibly via AKT and ERK pathways. A similar phenomenon was confirmed in macrophage Raw 264.7 cells. As shown in Figure S2, fullerol depicted dose-dependent effects on alleviating TNF-α-induced ERK and AKT phosphorylation and decreased the basal phosphorylation level of these proteins at a higher dose of 10 μM.

## DISCUSSION

Almost every person experiences back pain at some point in their lives. The etiologies vary widely from case-to-case with most cases being caused by mechanical compression on nerve roots by herniated disc materials. Such herniation initiates a cascade of inflammation leading to back pain that radiates to the hip and leg, known as lumbar radiculopathy. There is not a safe and effective therapy so far to tackle radiculopathy in the clinical setting. In our opinion, a desired therapy should at least address both inflammation and associated neuropathic pain during the onset of radiculopathy. Cytokines such as TNF-α participates in the genesis of inflammatory and neuropathic pain and elicits long-term mechanical allodynia in both naïve and nerve injury models. Exposure to TNF-α elevates sensitivity to capsaicin and increases TRPV1 sensitivity to heat and other stimuli in corresponding spinal DRGs. Hence, navigating TRPV-1 and its downstream functions may provide a unique opportunity to target inflammation and hypersensitivity. We have shown that fullerol attenuated TNF-α-induced neuroinflammation in mouse DRG and neurons and alleviated radicular pain in an NP implant mouse model.[4] To further understand molecular mechanisms of fullerol's analgesic effects in lumbar radiculopathy, we asked whether fullerol possesses any beneficial effects against TNF-α-elicited changes on TRPV-1 channels, intracellular $Ca^{2+}$ level, and activation of mitogen-activated protein kinase (MAPK) signaling in DRG neurons.

To address these questions, we first confirmed fullerol's analgesic effects in an anterior disc herniation radicular pain mouse model, which better mimics human lumbar radiculopathy than the NP implant model. Consistently, we demonstrated that a single and local application of 1 μM fullerol solution onto the disc herniation site could effectively attenuate ipsilateral hyperalgesia for up to 2 weeks (Figure 2C). Unlike the NP implant model, both ipsilateral and contralateral hind paws experience mechanical hyperalgesia; in this radicular pain model, the contralateral paw mechanical withdrawal threshold is not impacted, which is similar to human radiculopathy. Moreover, application of fullerol restored disc height and accelerated regeneration of disrupted extracellular matrix (Figure 3). These data suggested that fullerol could alleviate radicular pain and regenerate extracellular matrix of degenerated discs caused by injury-induced herniation.

In peripheral neuropathic pain, the primary sensory neurons residing within DRG are mainly responsible for pain transduction. Following disc herniation, a proinflammatory condition is therefore elicited by numerous inflammatory mediators that sensitize nociceptors and enhance pain. DRG neurons are a major source of increased nociceptive signaling through increased neuronal excitability.[43] Considerable research has focused on the vanilloid (V1) and ankyrin (A1) varieties of transient receptor potential (TRP) cation channels in sensory neurons because of their pivotal roles in the transduction of pain signals. It has been reported that, after damage to peripheral sensory fibers, upregulated expression of the Cavα2δ−1 channel subunit, the Nav1.3 sodium channel, and bradykinin (BK) B1 and TRPV1 receptors in myelinated neurons contribute to hyperalgesia.[44] TRPV1 is preferentially expressed in Aδ- and C-fiber nociceptors. It is possible that the inflammation-associated hyperalgesia produces not only an excessive release of pain mediators but also causes abnormally high levels of synaptic activity and pain sensitivity through upregulating the surface availability of these transducing channels. Others also reported that dopamine downregulates TRPV1

channels expressed in small diameter DRG neurons.[45] Indeed, we demonstrated that TNF-α stimulation significantly elevated expression of TRPV-1 in both small and medium neurons, which was effectively prevented by fullerol treatment to become even lower than the basal control level (Figure 4).

Calcium is an integral second messenger in neurons and is involved in the functional and structural neuronal plasticity that underlies peripheral and central sensitization at all levels. $Ca^{2+}$ triggers synaptic vesicle exocytosis, thus releasing the neurotransmitters contained in the vesicles and imitating synaptic transmission.[46] It has been a consensus that two prominent changes in DRG neurons in models of chronic inflammatory pain are increases in the basal concentration of cytosolic calcium ions and altered voltage-dependent calcium currents. Resting calcium levels in medium diameter sensory neurons, for example, were seen to be higher, and depolarization evoked calcium transients to be larger and to decay more slowly in small- and medium-diameter sensory neurons from inflamed tissues.[47] Our confocal calcium imaging data (Figure 5) suggested that, in both the presence and absence of TNF-α, fullerol significantly decreased intracellular calcium concentration. Because the contribution of increased calcium levels in DRG primary neurons to inflammatory hyperalgesia most likely results from the facilitation of transmitter release both in the periphery and at central terminals, fullerol possibly prevented TNF-α-sensitized neuronal excitability and pain through downregulating basal Ca level. Fullerol's protective effect against TNF-α-stimulated intracellular $Ca^{2+}$ level in DRG neurons provides an excellent opportunity for targeting primary sensory neurons to prevent the development of these pathological discharges. There are many different neurotransmitters that may be regulated by $Ca^{2+}$ channels, including amino acids, gasotransmitters, monaminines, trace amines, purines, and peptides. Future investigations might be carried out to elucidate fullerol's participation among complex interactions between $Ca^{2+}$ channels and neurotransmitters.

The neuropeptide substance P is commonly expressed in primary sensory neurons and is commonly regarded as a "pain" neurotransmitter.[48] CGRP, a pro-nociceptive neuropeptide, has been shown with increased synthesis and release in several types of neuropathic pain. Although we have shown that fullerol counteracts the upregulated expression of these neuropeptides in inflammatory cytokine TNF-α-stimulated DRGs, we did not investigate which cells were responsible for such effects.[21] By double immunofluorescent confocal imaging in the current work, we not only confirmed that fullerol counteracted TNF-α-stimulated overexpression of substance P and CGRP but also successfully detected that the majority of substance P- and CGRP-positive signals presented in small and medium neurons (Figure 6) based on neuron size analysis in Figure 4. Not surprisingly, neuropeptide-positive signals were also observed in other cells such as glial cells in response to environmental changes, which may in turn alter their neighboring neuronal function. Additionally, it has been documented that TNF-α-induced upregulation of CGRP and substance P synthesis involves MAPK pathways, such as ERK and AKT.[21,49] Consistently, our data here suggested that ERK and AKT are possibly responsible for observed fullerol's beneficial effect (Figure 7). Moreover, we also exhibited that fullerol significantly alleviated LPS-induced phosphorylation of ERK and AKT in Raw 264.7 macrophage model cells (Figure S2). These results might be supportive of a possible synergistic effect of fullerol in

antagonizing TNF-α-evoked inflammation and nociceptive pathways in both neuron and adjacent glia cells, both responsible for neuropathic pain.

Translational use of nanofullerol in treating lumbar radiculopathy and any other pathological conditions should involve careful investigation of toxicity issues. Typically, at low dose, fullerol has shown no detectable levels of toxicity when administered intravenously in rats.[50] In vitro assays have proven that fullerol is a nontoxic compound capable of tiny amounts of ROS generation without causing significant harm or potential toxicity.[51] In addition, fullerol has a half-life in systemic circulation reported at least 1 week postinjection in animals with most accumulation presenting in the liver.[52] The feature of long circulation may act as a double-edge sword for either prolonging the therapeutic effect or difficulty in clearing from the body, and a more thorough study regarding this issue shall be performed, in particular to address the chronic effect of fullerol with additional attention on formation, material characterization, and route of in vivo administration.

## CONCLUSIONS

Our study demonstrated the therapeutic potential of biocompatible nanofullerol in a clinically relevant mouse model of lumbar radiculopathy, which might be mediated through downregulating the pro-inflammatory cytokine TNF-α-induced ion channel activation, calcium ion homeostasis, and neuropeptide production in DRG and neurons via AKT and ERK pathways. These results provide a unique preclinical foundation for fullerol leaping forward to further translational investigations.

## Supplementary Material

Refer to Web version on PubMed Central for supplementary material.

## Acknowledgments

This work was supported by funding from the National Institute of Arthritis and Musculoskeletal and Skin Disease of the U.S. National Institutes of Health (R01AR064792 and R21AR057512), North American Spine Society, and Department of Orthopaedic Surgery, University of Virginia, all to X.L.

## References

1Morry J, Ngamcherdtrakul W, Yantasee W. Oxidative stress in cancer and fibrosis: Opportunity for therapeutic intervention with antioxidant compounds, enzymes, and nanoparticles. Redox Biol. 2017; 11:240–253. [PubMed: 28012439]

2Yin J-J, Lao F, Fu PP, Wamer WG, Zhao Y, Wang PC, Qiu Y, Sun B, Xing G, Dong J, Liang X-J, Chen C. The scavenging of reactive oxygen species and the potential for cell protection by functionalized fullerene materials. Biomaterials. 2009; 30(4):611–621. [PubMed: 18986699]

3Liu Q, Jin L, Mahon BH, Chordia MD, Shen FH, Li X. A Novel Treatment of Neuroinflammation against Low Back Pain by Soluble Fullerol Nanoparticles. Spine. 2013; 38(17):1443–1451. [PubMed: 23466506]

4Jin L, Ding M, Oklopcic A, Aghdasi B, Xiao L, Li Z, Jevtovic-Todorovic V, Li X. Nanoparticle fullerol alleviates radiculopathy via NLRP3 inflammasome and neuropeptides. Nanomedicine. 2017; 13(6):2049–2059. [PubMed: 28404518]

5Hoy D, March L, Brooks P, Blyth F, Woolf A, Bain C, Williams G, Smith E, Vos T, Barendregt J, Murray C, Burstein R, Buchbinder R. The global burden of low back pain: estimates from the Global Burden of Disease 2010 study. Ann Rheum Dis. 2014; 73(6):968–74. [PubMed: 24665116]

6Andersson GBJ. Epidemiological features of chronic low-back pain. Lancet. 1999; 354(9178):581–585. [PubMed: 10470716]

7Kepler CK, Ponnappan RK, Tannoury CA, Risbud MV, Anderson DG. The molecular basis of intervertebral disc degeneration. Spine J. 2013; 13(3):318–330. [PubMed: 23537454]

8Jin L, Feng G, Reames DL, Shimer AL, Shen FH, Li X. The Effects of Simulated Microgravity on Intervertebral Disc Degeneration. Spine J. 2013; 13(3):235–242. [PubMed: 23537452]

9Belavý DL, Albracht K, Bruggemann G-P, Vergroesen P-PA, van Dieën JH. Can Exercise Positively Influence the Intervertebral Disc? Sports Med. 2016; 46(4):473–485. [PubMed: 26666742]

10Guterl CC, See EY, Blanquer SBG, Pandit A, Ferguson SJ, Benneker LM, Grijpma DW, Sakai D, Eglin D, Alini M, Iatridis JC, Grad S. Challenges and stratigies in the repair of ruptured annulus fibrosus. Eur Cell Mater. 2013; 25:1–21. [PubMed: 23283636]

11Bhatia A, Flamer D, Shah PS, Cohen SP. Transforaminal Epidural Steroid Injections for Treating Lumbosacral Radicular Pain from Herniated Intervertebral Discs: A Systematic Review and Meta-Analysis. Anesth Analg. 2016; 122(3):857–870. [PubMed: 26891397]

12Biddie SC, , Conway-Campbell BL, , Lightman SL. Rheumatology Vol. 51. Oxford, U. K: 2012 Dynamic regulation of glucocorticoid signalling in health and disease; 403412

13Leung L, Cahill CM. TNF-α and neuropathic pain – a review. J Neuroinflammation. 2010; 7:27–27. [PubMed: 20398373]

14Feldmann M, Maini RN. TNF defined as a therapeutic target for rheumatoid arthritis and other autoimmune diseases. Nat Med. 2003; 9(10):1245–1250. [PubMed: 14520364]

15Mattei RA, Dalmarco EM, Fröde TS. Etanercept administration prevents the inflammatory response induced by carrageenan in the murine air pouch model. Naunyn-Schmiedeberg's Arch Pharmacol. 2015; 388(12):1247–1257. [PubMed: 26255064]

16Isyar M, Bilir B, Yilmaz I, Cakmak S, Sirin DY, Guzelant AY, Mahirogullari M. Are biological agents toxic to human chondrocytes and osteocytes? J Orthop Surg Res. 2015; 10:118. [PubMed: 26223355]

17Kübra Elçioğlu H, Kabasakal L, Tufan F, Elçioğlu ÖH, Solakoglu S, Kotil T, Karan MA. Effects of systemic Thalidomide and intracerebroventricular Etanercept and Infliximab administration in a Streptozotocin induced dementia model in rats. Acta Histochem. 2015; 117(2):176–181. [PubMed: 25596877]

18Lories RJ, de Vlam K. Tumour necrosis factor inhibitors in the treatment of psoriatic arthritis: a view on effectiveness, clinical practice and toxicity. Expert Opin Biol Ther. 2014; 14(12):1825–1836. [PubMed: 25366335]

19Yang X, Jin L, Yao L, Shen FH, Shimer AL, Li X. Antioxidative nanofullerol prevents intervertebral disk degeneration. Int J Nanomed. 2014; 9:2419–2430.

20Arifa RDN, Paula TPd, Madeira MFM, Lima RL, Garcia ZM, ÿvila TV, Pinho V, Barcelos LS, Pinheiro MVB, Ladeira LO, Krambrock K, Teixeira MM, Souza DG. The reduction of oxidative stress by nanocomposite Fullerol decreases mucositis severity and reverts leukopenia induced by Irinotecan. Pharmacol Res. 2016; 107:102–110. [PubMed: 26987941]

21Xiao L, Ding M, Fernandez A, Zhao P, Jin L, Li X. Curcumin alleviates lumbar radiculopathy by reducing neuroinflammation, oxidative stress and nociceptive factors. Eur Cell Mater. 2017; 33:279–293. [PubMed: 28485773]

22Bonin RP, Bories C, De Koninck Y. A simplified up-down method (SUDO) for measuring mechanical nociception in rodents using von Frey filaments. Mol Pain. 2014; 10:26–26. [PubMed: 24739328]

23Xiao L, Ding M, Zhang Y, Chordia M, Pan D, Shimer A, Shen F, Glover D, Jin L, Li X. A Novel Modality for Functional Imaging in Acute Intervertebral Disk Herniation via Tracking Leukocyte Infiltration. Mol Imaging Biol. 2017; 19(5):703–713. [PubMed: 28050750]

24Walter BA, Torre OM, Laudier D, Naidich TP, Hecht AC, Iatridis JC. Form and function of the intervertebral disc in health and disease: a morphological and stain comparison study. J Anat. 2015; 227(6):707–716. [PubMed: 25424497]

25Malin SA, Davis BM, Molliver DC. Production of dissociated sensory neuron cultures and considerations for their use in studying neuronal function and plasticity. Nat Protocols. 2007; 2(1): 152–160. [PubMed: 17401349]

26Xiao L, Ding M, Saadoon O, Vess E, Fernandez A, Zhao P, Jin L, Li X. A novel culture platform for fast proliferation of human annulus fibrosus cells. Cell Tissue Res. 2017; 367(2):339–350. [PubMed: 27623803]

27Hoffman EM, Zhang Z, Schechter R, Miller KE. Glutaminase Increases in Rat Dorsal Root Ganglion Neurons after Unilateral Adjuvant-Induced Hind Paw Inflammation. Biomolecules. 2016; 6(1):10. [PubMed: 26771651]

28Zhang M-D, Tortoriello G, Hsueh B, Tomer R, Ye L, Mitsios N, Borgius L, Grant G, Kiehn O, Watanabe M, Uhlén M, Mulder J, Deisseroth K, Harkany T, Hökfelt TGM. Neuronal calcium-binding proteins 1/2 localize to dorsal root ganglia and excitatory spinal neurons and are regulated by nerve injury. Proc Natl Acad Sci USA. 2014; 111(12):E1149–E1158. [PubMed: 24616509]

29Sonkusare SK, , Bonev AD, , Ledoux J, , Liedtke W, , Kotlikoff MI, , Heppner TJ, , Hill-Eubanks DC, , Nelson MT. Science Vol. 336. Washington, DC, U. S: 2012 Elementary Ca2+ signals through endothelial TRPV4 channels regulate vascular function; 597601

30Sonkusare SK, Dalsgaard T, Bonev AD, Nelson MT. Inward rectifier potassium (Kir2.1) channels as end-stage boosters of endothelium-dependent vasodilators. J Physiol. 2016; 594(12):3271–3285. [PubMed: 26840527]

31Woodruff ML, Sampath AP, Matthews HR, Krasnoperova NV, Lem J, Fain GL. Measurement of cytoplasmic calcium concentration in the rods of wild-type and transducin knockout mice. J Physiol. 2002; 542(Pt 3):843–854. [PubMed: 12154183]

32Dunn KM, Hill-Eubanks DC, Liedtke WB, Nelson MT. TRPV4 channels stimulate Ca2+-induced Ca2+ release in astrocytic endfeet and amplify neurovascular coupling responses. Proc Natl Acad Sci USA. 2013; 110(15):6157–6162. [PubMed: 23530219]

33Gruber HE, Ingram J, Hanley EN Jr. An improved staining method for intervertebral disc tissue. Biotech Histochem. 2002; 77(2):81–83. [PubMed: 12083388]

34Suzuki H, Aoyama Y, Senzaki K, Vincler M, Wittenauer S, Yoshikawa M, Ozaki S, Oppenheim RW, Shiga T. Characterization of sensory neurons in the dorsal root ganglia of Bax-deficient mice. Brain Res. 2010; 1362:23–31. [PubMed: 20846512]

35Gunthorpe MJ, Benham CD, Randall A, Davis JB. The diversity in the vanilloid (TRPV) receptor family of ion channels. Trends Pharmacol Sci. 2002; 23(4):183–191. [PubMed: 11931994]

36Pamarthi MF, Rudd MA, Bukoski RD. Normal perivascular sensory dilator nerve function in arteries of Zucker diabetic fatty rats. Am J Hypertens. 2002; 15(4 Pt 1):310–315. [PubMed: 11991215]

37Heath MJ, Womack MD, MacDermott AB. Substance P elevates intracellular calcium in both neurons and glial cells from the dorsal horn of the spinal cord. J Neurophysiol. 1994; 72(3):1192–1198. [PubMed: 7528792]

38Rozas P, Lazcano P, Pina R, Cho A, Terse A, Pertusa M, Madrid R, Gonzalez-Billault C, Kulkarni AB, Utreras E. Targeted overexpression of tumor necrosis factor-alpha increases cyclin-dependent kinase 5 activity and TRPV1-dependent Ca2+ influx in trigeminal neurons. Pain. 2016; 157(6): 1346–1362. [PubMed: 26894912]

39Ringer C, Tune S, Bertoune MA, Schwarzbach H, Tsujikawa K, Weihe E, Schütz B. Disruption of calcitonin gene-related peptide signaling accelerates muscle denervation and dampens cytotoxic neuroinflammation in SOD1 mutant mice. Cell Mol Life Sci. 2017; 74:1–20. [PubMed: 27704173]

40Takahashi N, Kikuchi S, Shubayev VI, Campana WM, Myers RR. TNF-alpha and phosphorylation of ERK in DRG and spinal cord: insights into mechanisms of sciatica. Spine. 2006; 31(5):523–529. [PubMed: 16508545]

41Lin YT, Ro LS, Wang HL, Chen JC. Up-regulation of dorsal root ganglia BDNF and trkB receptor in inflammatory pain: an in vivo and in vitro study. J Neuroinflammation. 2011; 8:126. [PubMed: 21958434]

42Park CK, Lu N, Xu ZZ, Liu T, Serhan CN, Ji RR. Resolving TRPV1- and TNF-alpha-mediated spinal cord synaptic plasticity and inflammatory pain with neuroprotectin D1. J Neurosci. 2011; 31(42):15072–15085. [PubMed: 22016541]

43Sapunar D, Kostic S, Banozic A, Puljak L. Dorsal root ganglion − a potential new therapeutic target for neuropathic pain. J Pain Res. 2012; 5:31–38. [PubMed: 22375099]

44Hagenston AM, Simonetti M. Neuronal calcium signaling in chronic pain. Cell Tissue Res. 2014; 357(2):407–426. [PubMed: 25012522]

45Chakraborty S, Rebecchi M, Kaczocha M, Puopolo M. Dopamine modulation of transient receptor potential vanilloid type 1 (TRPV1) receptor in dorsal root ganglia neurons. J Physiol. 2016; 594(6):1627–1642. [PubMed: 26563747]

46Sudhof TC. Calcium control of neurotransmitter release. Cold Spring Harbor Perspect Biol. 2012; 4(1):a011353.

47Lu SG, Gold MS. Inflammation-induced increase in evoked calcium transients in subpopulations of rat dorsal root ganglion neurons. Neuroscience. 2008; 153(1):279–288. [PubMed: 18367340]

48Jo YY, Lee JY, Park C-K. Resolvin E1 Inhibits Substance P-Induced Potentiation of TRPV1 in Primary Sensory Neurons. Mediators Inflammation. 2016; 2016:5259321.

49Lin Y-T, Ro L-S, Wang H-L, Chen J-C. Up-regulation of dorsal root ganglia BDNF and trkB receptor in inflammatory pain: an in vivo and in vitro study. J Neuroinflammation. 2011; 8:126–126. [PubMed: 21958434]

50Monteiro-Riviere NA, Linder KE, Inman AO, Saathoff JG, Xia X-R, Riviere JE. Lack of Hydroxylated Fullerene Toxicity after Intravenous Administration to Female Sprague-Dawley Rats. J Toxicol Environ Health, Part A. 2012; 75(7):367–373. [PubMed: 22524592]

51Xia T, Kovochich M, Brant J, Hotze M, Sempf J, Oberley T, Sioutas C, Yeh JI, Wiesner MR, Nel AE. Comparison of the Abilities of Ambient and Manufactured Nanoparticles To Induce Cellular Toxicity According to an Oxidative Stress Paradigm. Nano Lett. 2006; 6(8):1794–1807. [PubMed: 16895376]

52Yamago S, Tokuyama H, Nakamura E, Kikuchi K, Kananishi S, Sueki K, Nakahara H, Enomoto S, Ambe F. In vivo biological behavior of a water-miscible fullerene: 14C labeling, absorption, distribution, excretion and acute toxicity. Chem Biol. 1995; 2(6):385–389. [PubMed: 9383440]

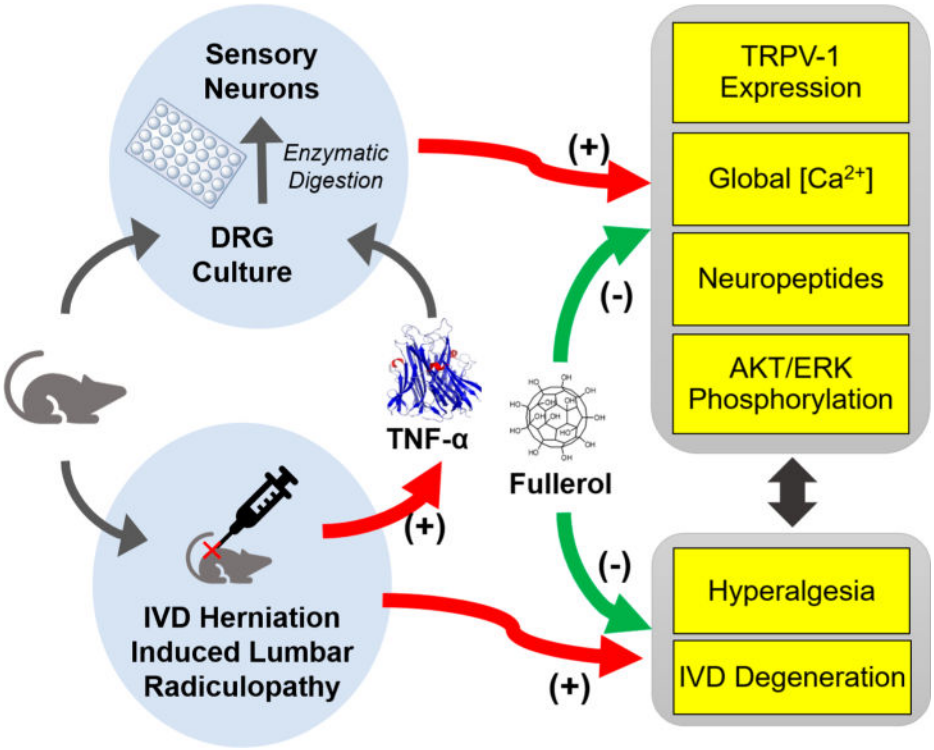


**Figure 1.**

Schematic and mechanistic hypothesis of fullerol's therapeutic potential against lumbar radiculopathy secondary to disc herniation: (1) in vitro pleiotropic functions via attenuating TNF-α-induced neuroinflammation and alternation in nociceptive factors, ion channel, intracellular [$Ca^{2+}$], and signaling pathways in DRG and/or primary sensory neurons, and (2) in vivo analgesic effect in a clinically relevant mouse model of lumbar radiculopathy secondary to disc herniation.

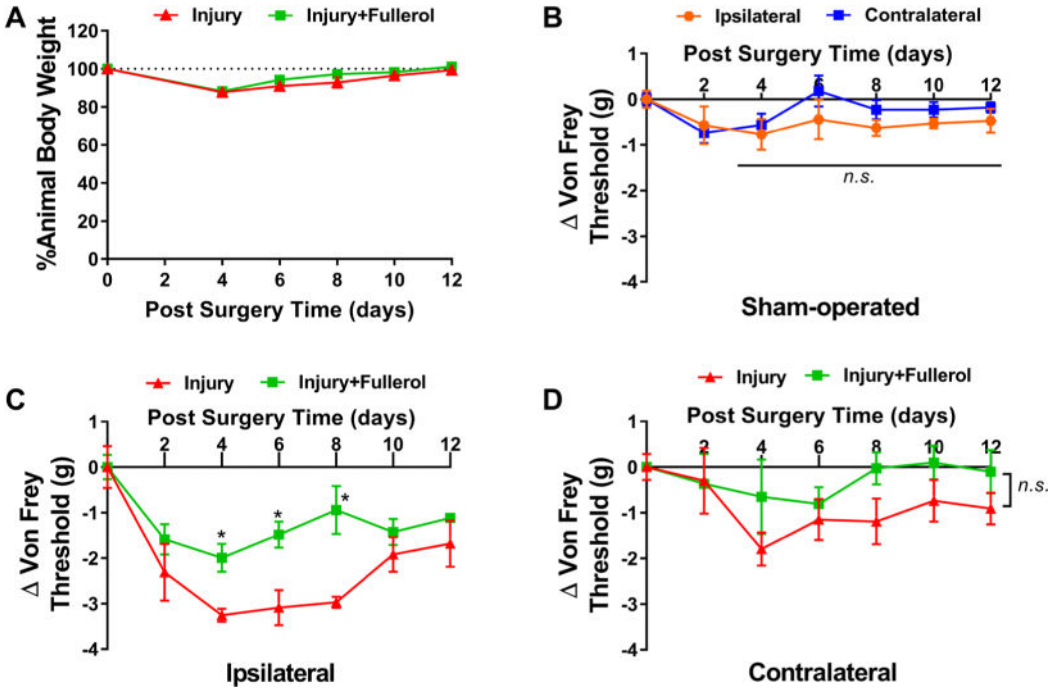


**Figure 2.**

Fullerol alleviates the ipsilateral mechanical hyperalgesia in a mouse model of lumbar radiculopathy induced by disc herniation. (A) Steadily recovering animal body weights after POD4 indicate an overall good recovery of tested animals. (B) In a sham-operated animal group, no significant difference in mechanical sensitivity is observed in both ipsilateral and contralateral sides after surgery up to POD12. (C) Intraoperative administration of fullerol solution (1 $\mu$M, 10 $\mu$L per 20 g of body weight) restores ipsilateral mechanical hyperalgesia secondary to disc herniation in mice up to POD12 using the electronic von Frey method, whereas neither the disc injury nor the fullerol treatment significantly alters the mechanical threshold on the contralateral side (D). Saline was used in the injury-only group as a control vehicle. Five mice were used in each group.

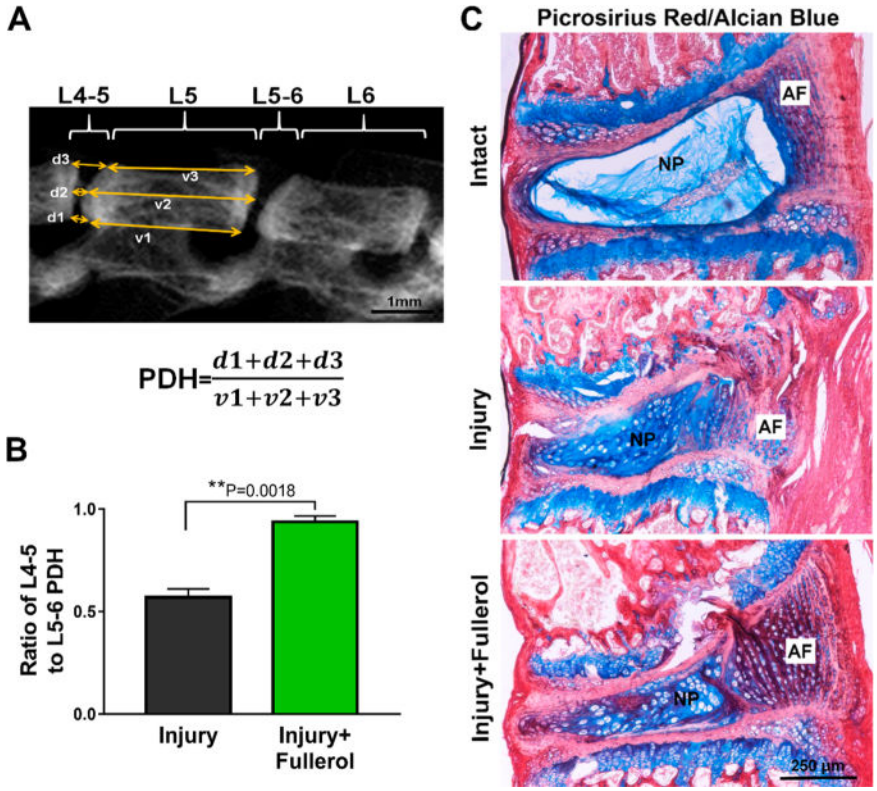


**Figure 3.**

Fullerol possesses a potential regenerative effect in a mouse disc herniation model. (A) Representative microCT image of mouse spine at 2 weeks after surgery indicates that fullerol restores disc height of injured IVD. (B) The injury + fullerol group shows an increase in the ratio of L4–5 to L5–6 PDH ($^{**}p = 0.0018$). (C) Alcian blue/picrosirius red staining confirms degenerative change and an ongoing regenerative process of injured IVD postfullerol treatment. After 2 weeks postsurgery, compared to intact disc (top row), injury + saline (middle row) discs demonstrate classical manifestations of disc degeneration such as ruptured AF lamina, enlarged and proliferated chondrocytes, disappearing distinctive boundary between AF and NP, and damaged end plates. The fullerol-treated group (bottom row) exhibits much stronger purple staining in the inner AF and red staining in the outer AF regions, suggesting an active regenerative process of newly formed proteoglycan and collagen, respectively. Scale bar = 250 $\mu$m. Five mice were used in each group.

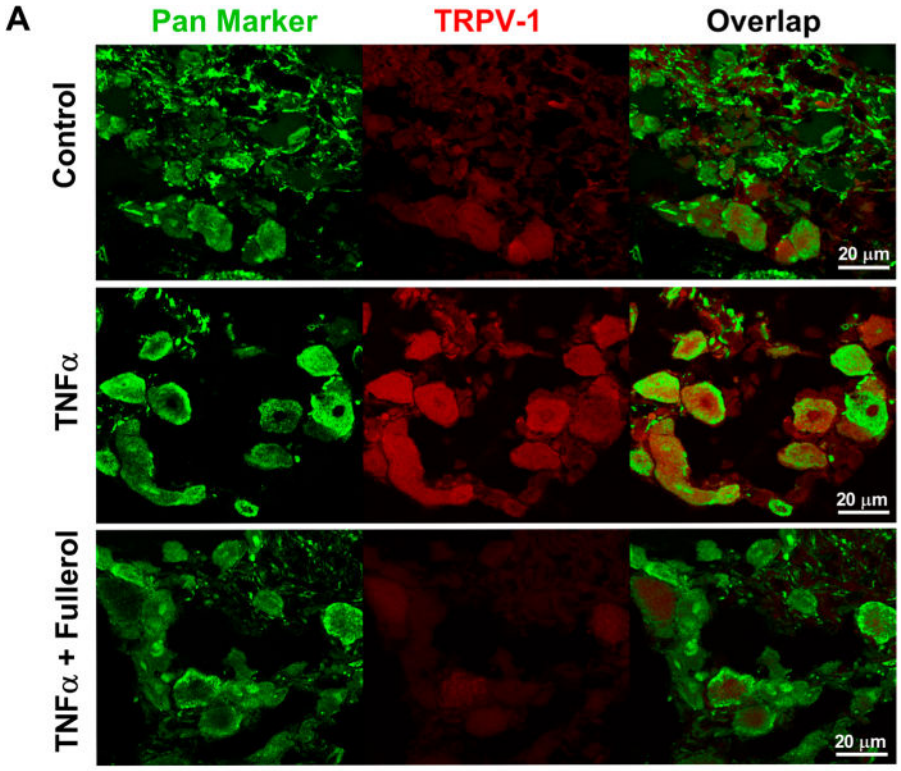


B

| DRG Neuron Counts | Small <300 μm² | | Medium 300-700 μm² | | Large >700 μm² | | Total | |
|---|---|---|---|---|---|---|---|---|
| | Pan | TRPV-1 | Pan | TRPV-1 | Pan | TRPV-1 | Pan | TRPV-1 |
| Control | 404 | 95 | 200 | 34 | 19 | 0 | 623 | 129 |
| TNFα | 617 | 264 | 190 | 73 | 7 | 3 | 814 | 340 |
| TNFα+Fullerol | 531 | 45 | 171 | 45 | 17 | 0 | 719 | 90 |

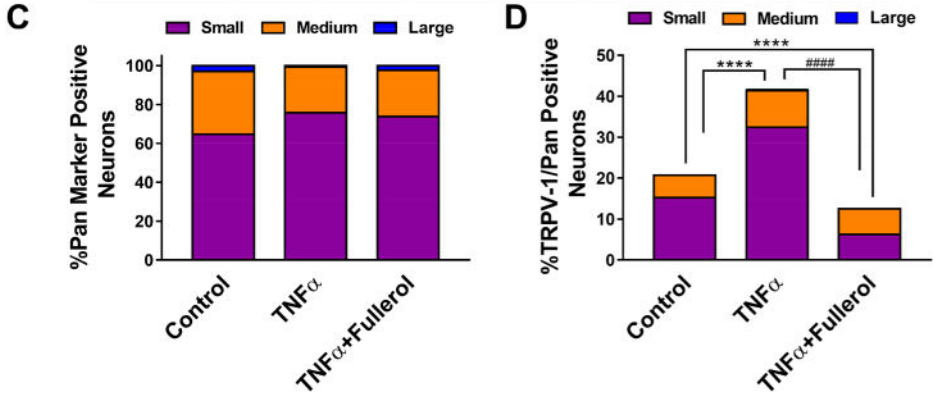


**Figure 4.**

Fullerol attenuates TNF-α-elicited TPRV-1 expression in DRG neurons. (A) Representative confocal immunofluorescence images of DRG (Pan neuron, green; TRPV-1, red) suggests TNF-α upregulates TRPV-1 expression, whereas fullerol (1 $\mu$M) treatment counters such enhancement after 24 h. (B) Summary of all sizes of neurons (small, <300 $\mu m^2$; medium, 300–700 $\mu m^2$; large, >700 $\mu m^2$) analyzed in the current study based on cross-sectional area ($\mu m^2$) highlighted by Pan neuron marker. (C) Percentage of size distribution of Pan-positive neurons in each treatment group. (D) Quantitative analysis showing TRPV-1/neuron size is significantly increased in the TNF-α group, which is alleviated by 1 $\mu$M fullerol. ****$p <$

0.0001 vs control; $^{\#\#\#\#}p < 0.0001$ vs TNF-α. Scale bar = 20 μm. Three sections per DRG; 7–10 DRGs per group were analyzed.

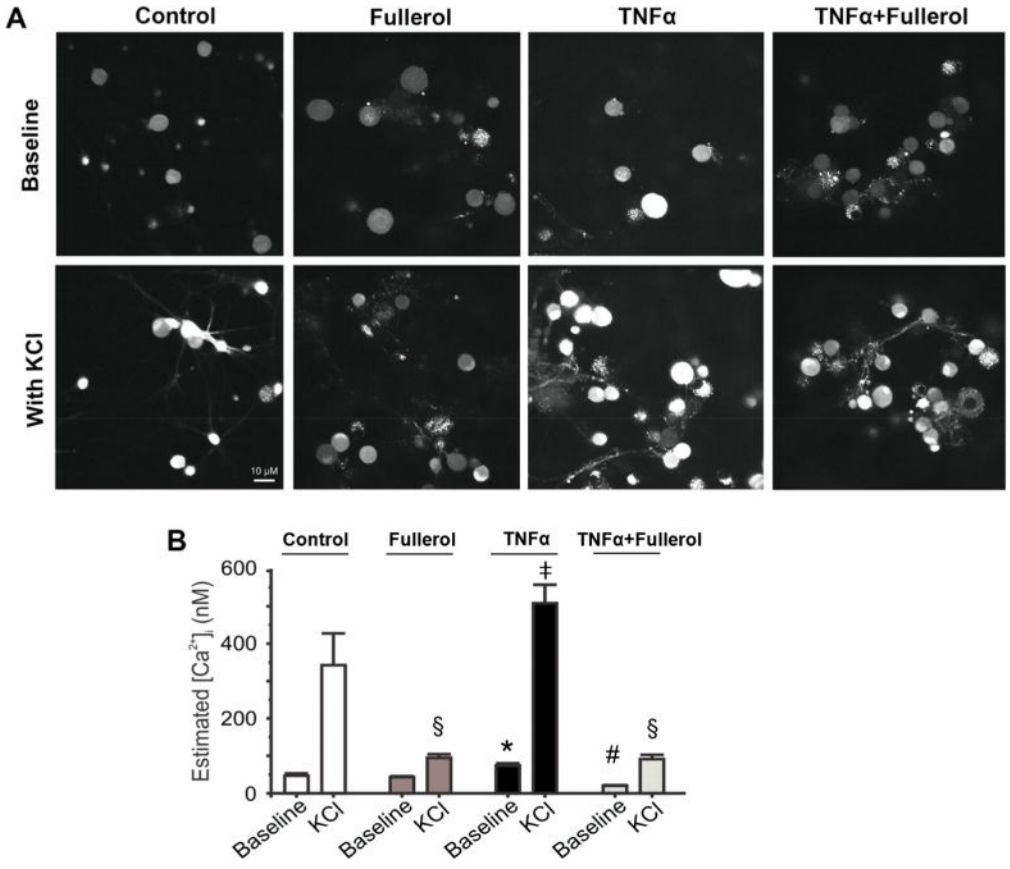


**Figure 5.**

Fullerol abolishes the TNF-$\alpha$-induced increase in $[Ca^{2+}]_i$ in primary DRG neurons. (A) Representative images showing intracellular $Ca^{2+}$ fluorescence of primary DRG neurons pretreated with F-12 media (control), fullerol (1 $\mu$M), TNF-$\alpha$ (10 ng/mL), or TNF-$\alpha$ (10 ng/mL) + fullerol (1 $\mu$M) overnight in the absence (upper row) or presence (lower row) of 60 mM KCl. (B) Nanofullerol neutralizes the increase in estimated intracellular $Ca^{2+}$ concentration ($[Ca^{2+}]_i$) induced by TNF-$\alpha$. Whereas neurons treated exclusively with TNF-$\alpha$ lead to higher $[Ca^{2+}]_i$, those treated with fullerol and TNF-$\alpha$ + fullerol show significantly lower global ($[Ca^{2+}]_i$). KCl-stimulated elevations in $[Ca^{2+}]_i$ are also reduced by pretreating with fullerol. For baseline, $p < 0.05$, *TNF-$\alpha$ vs control, fullerol, and TNF-$\alpha$ + fullerol; #TNF-$\alpha$ + fullerol vs control, fullerol, and TNF-$\alpha$. For KCl treated, $p < 0.05$, §Fullerol vs control; ‡TNF-$\alpha$ vs fullerol and TNF-$\alpha$ + fullerol. Data are presented as mean ± SEM; 20–30 neurons were analyzed per group.

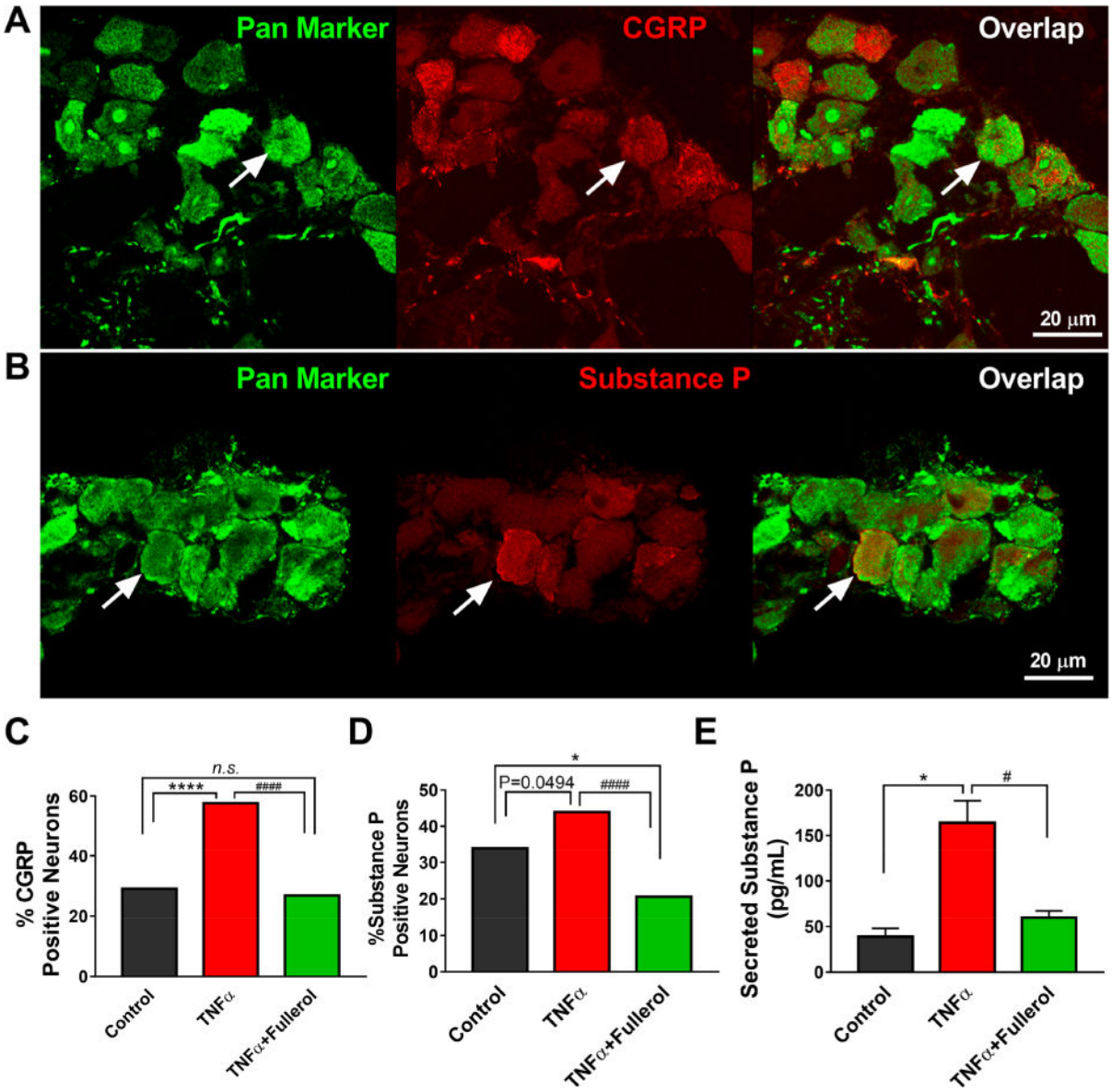


**Figure 6.**

Fullerol (1 $\mu$M) attenuated TNF-α-elicited expression of substance P and CGRP in DRG explant culture. Representative immunofluorescent staining suggested increased expression of CGRP (A) and substance P (B) by TNF-α (25 ng/mL) in DRG neurons after 24 h incubation. (C, D) Quantitative analysis of percentages of substance P and CGRP in DRG neurons. (E) ELISA assay confirmed that fullerol (1 $\mu$M) attenuated TNF-α-promoted (25 ng/mL) substance P release in DRG culture media after 24 h treatment. *$p < 0.05$, ****$p < 0.0001$ vs control; $^{\#}p < 0.05$ and $^{\#\#\#\#}p < 0.0001$ vs TNF-α. Scale bar = 20 $\mu$m. Three sections per DRG and ~7 DRGs per group were analyzed.

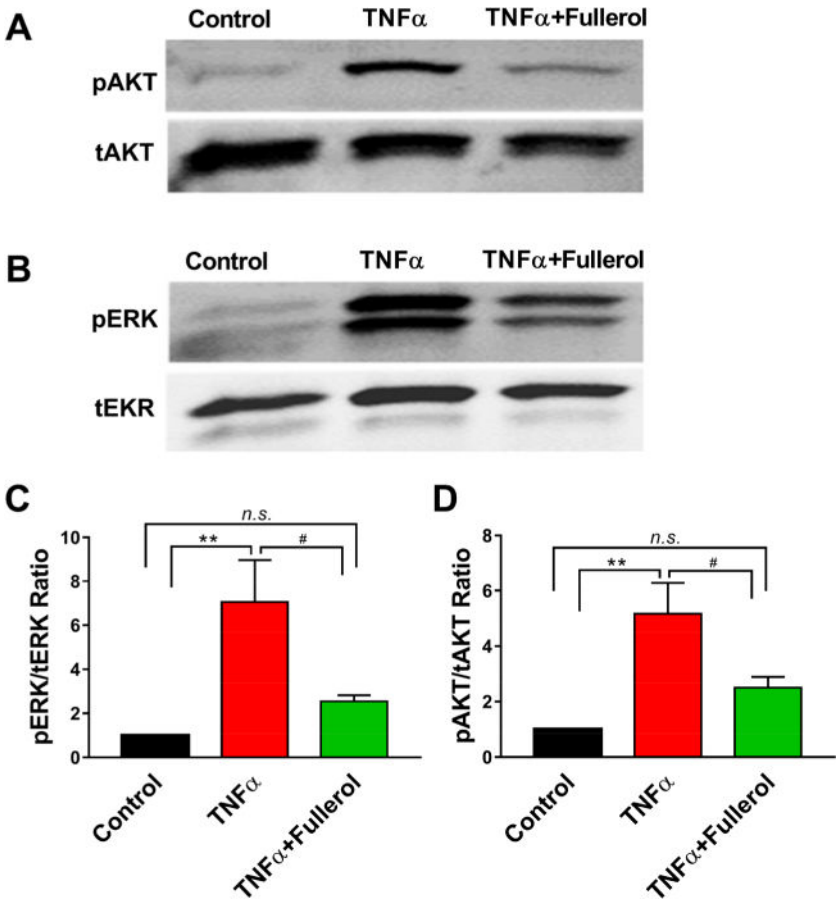


**Figure 7.**

Fullerol alleviated TNF-α-induced neuroinflammation in mouse DRG explants. At 5 h post treatment, fullerol (1 μM) prevented TNF-α-induced phosphorylation of AKT (A, D) and ERK (B, C) as detected by Western blotting and quantified via densitometry analysis. $^{**}p <$ 0.005 vs control; $^{\#}p < 0.05$, $^{\#\#}p < 0.005$ vs TNF-α. $n = 6$ groups of DRGs (5–6 DRGs per group) for each experiment.